Check for updates

# Concurrent tandem catalysis enabled by nanomechanical motion in heteroleptic four-component dual-catalyst machinery†

Emad Elramadi, [ID] ‡ Sohom Kundu,‡ Debabrata Mondal and Michael Schmittel [ID] *

When the basic ligand 3 was added to the heteroleptic three-component slider-on-deck $[Ag_3(1)(2)]^{3+}$ (sliding frequency $k_{298}$ = 57 kHz), it operated as a moderate brake pad ($k_{298}$ = 45 kHz). Due to motion in the resulting four-component slider-on-deck $[Ag_3(1)(2)(3)]^{3+}$, both ligand 3 and silver(I) were continuously exposed and became catalytically active in a concurrent tandem Michael addition/hydroalkoxylation.

Inside multicellular organisms, enzymes catalyze a gamut of reactions, ranging from simple to cascaded[1] and concurrent tandem reactions.[2] In many cases, enzymatic activity critically depends on protein mobility, *e.g.*, for substrate binding or product release.[3] If enzymes with multiple components are concerned, then mobility may even involve cooperative motions of distinct parts for achieving rate and efficiency increase,[4,5] as convincingly demonstrated by the ATP synthase.[6]

Only recently, chemists have been able to mimic such spectacular enzyme capabilities by developing multicomponent catalysts,[7–9] but few have succeeded to connect catalytic function with intrinsic motion.[10] Herein, we illustrate the suitability of four-component machinery to act as a dual catalytic effector for concurrent tandem catalysis with both processes occurring in one solution. Dual catalytic activity of a single slider-on-deck – instigated only by its dynamics – has not yet been realized.[11]

In earlier work, we demonstrated that the superior action of nanorotors and slider-on-deck systems as catalysts in both base-[12] or metal-catalyzed[13] reactions depended crucially on their motional speed. Notably, the speed correlated with the ability of the machinery to free the catalyst[12] or product[13] (reducing product inhibition). Such effect is conceptually different from static liberation of a catalyst as used in switchable catalysis.[14,15]

In detail, the four-component slider-on-deck was constructed from deck 1,[16] biped 2, silver(I) ions and the chelating base 3 as shown in Scheme 1 (for synthesis, see ESI,† Chapter 1). The resulting catalytic machinery $[Ag_3(1)(2)(3)]^{3+}$ exhibited a stochastic sliding motion that in parallel liberated the silver(I) sites and base 3 for catalysis. The resulting dual-catalyst machinery proved to be
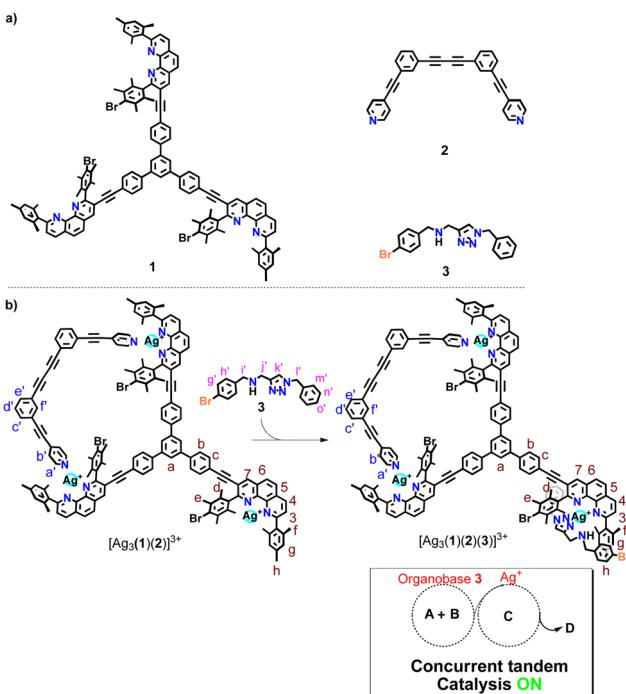


**Scheme 1** (a) Chemical structure of ligands 1–3. (b) Transformation of the three- into the four-component dual-catalyst machinery. Both organobase 3 and the silver(I) centers are liberated due to the sliding motion in $[Ag_3(1)(2)(3)]^{3+}$, which enables concurrent tandem catalysis. A & B represent the substrates, C denotes the intermediate product and D the final product of the concurrent tandem reaction.

*Center of Micro and Nanochemistry and (Bio)Technology, Organische Chemie I, School of Science and Technology, University of Siegen, Adolf-Reichwein-Str. 2, Siegen D-57068, Germany. E-mail: schmittel@chemie.uni-siegen.de; Tel: +49(0) 2717404356*

**Scheme 2** (a) Parallel one-pot base-catalyzed Michael addition and silver(I)-catalyzed cyclization. For catalyst(s), see Tables 1 and 2. (b) Sequential Michael addition/hydroalkoxylation reaction (for mechanism, see ESI,† Scheme S4).[17] (c) Further ligands used in this study.



**Fig. 1** Partial $^1$H NMR (600 MHz, CD$_2$Cl$_2$, 298 K) of silver(I)-loaded deck $[\mathrm{Ag}_3(\mathbf{1})]^{3+}$, slider-on-deck $[\mathrm{Ag}_3(\mathbf{1})(\mathbf{2})]^{3+}$ and biped **2**.

active in concurrent tandem base and silver(I)-catalyzed reactions, while dual catalysis in static reference structures was minor.

Before designing the main system, model studies were required to warrant the operation of the catalytic machinery. Thus, the chelating amine **3** and AgBF$_4$ were mixed in 1:1 and 2:1 ratio to investigate their combined catalytic activity. At a ratio of 1:1, $^1$H NMR spectroscopy showed formation of complex $[\mathrm{Ag}(\mathbf{3})]^+$. In case of a 2:1 ratio, the bishomoleptic complex $[\mathrm{Ag}(\mathbf{3})_2]^+$ was furnished (ESI,† Fig. S16).

To check the potential of both silver complexes to concurrently perform the base-catalyzed Michael addition $\mathbf{4} + \mathbf{5} \rightarrow \mathbf{6}$ and the silver(I)-catalyzed cyclization of $\mathbf{7} \rightarrow \mathbf{8}$ (Scheme 2), we mixed **4**, **5** and **7** in CD$_2$Cl$_2$ in presence of the silver(I) complex (either $[\mathrm{Ag}(\mathbf{3})]^+$ or $[\mathrm{Ag}(\mathbf{3})_2]^+$) at a ratio 10:10:10:1. At room temperature (for time, see Table 1) the Michael addition catalyzed by base **3** afforded only small amounts of **6**. The yields (11% vs. 13%) were similar although in $[\mathrm{Ag}(\mathbf{3})_2]^+$ the base concentration formally was 2-fold the one in $[\mathrm{Ag}(\mathbf{3})]^+$. In contrast, the yield of the silver(I)-catalyzed reaction was high with $[\mathrm{Ag}(\mathbf{3})]^+$ and ca. 8-fold less with $[\mathrm{Ag}(\mathbf{3})_2]^+$ (Table 1).

Further investigation with $[\mathrm{Ag}(\mathbf{3})]^+$ or $[\mathrm{Ag}(\mathbf{3})_2]^+$ as catalyst toward the concurrent tandem reaction of **4** and **9** (in a ratio 1:10:10) affording **10** (Scheme 2b and Table 1) revealed 4% and 11% yield of **10** after 14 h, respectively, and in case of $[\mathrm{Ag}(\mathbf{3})_2]^+$ only a minor increase of the yield after 40 h, i.e., to 17% (ESI,† Fig. S32–S35). Thus, high dual catalytic activity cannot be realized by simply combining chelating base **3** and silver ions.

We carried out further model studies to predict the catalytic strength of the final assembly $[\mathrm{Ag}_3(\mathbf{1})(\mathbf{2})(\mathbf{3})]^{3+}$, if it were static! Thus, benzyl amine **3**, AgBF$_4$, 2,9-dimesitylphenanthroline (**11**) and 4-iodopyridine (**12**) were mixed in a 1:3:3:2 ratio to furnish $2 \times [\mathrm{Ag}(\mathbf{11})(\mathbf{12})]^+ + [\mathrm{Ag}(\mathbf{3})(\mathbf{11})]^+$, reflecting the three coordination units in the assembly $[\mathrm{Ag}_3(\mathbf{1})(\mathbf{2})(\mathbf{3})]^{3+}$. While silver catalysis was ON, base catalysis was completely OFF (ESI,† Table S1). Apparently, base **3** remains strongly bound to $[\mathrm{Ag}(\mathbf{11})]^+$ as the binding constant is $\log K = 5.96$ (see ESI,† Fig. S45). Hence, the question emerged, whether the motion of biped **2** in the slider-on-deck $[\mathrm{Ag}_3(\mathbf{1})(\mathbf{2})(\mathbf{3})]^{3+}$ would lead to a steady exposure of both the base and silver(I)-ions thus setting up a dual-catalyst machinery for concurrent tandem reactions.

Upon mixing **1**, **2** and silver(I) in 1:1:3 ratio at room temperature in CD$_2$Cl$_2$, the three-component slider-on-deck immediately self-assembled in quantitative yield, as evidenced by NMR and mass spectroscopy. The $^1$H NMR of $[\mathrm{Ag}_3(\mathbf{1})(\mathbf{2})]^{3+}$ shows a single signal set as both pyridine feet of biped **2** are sliding across all three silver(I) phenanthroline units of deck $[\mathrm{Ag}_3(\mathbf{1})]^{3+}$. Since the pyridine feet of **2** are placed between the shielding phenanthroline's aryl groups, diagnostic upfield shifts are seen for proton signals a′-H and b′-H from 8.62 and 7.38 ppm in **2** to 6.84 and 7.32 ppm, respectively, despite their binding to the silver(I) ions. In contrast to the inner deck's proton signals, i.e., a-, b- and c-H, that remained constant, most phenanthroline signals are slightly shifted downfield when compared to those in $[\mathrm{Ag}_3(\mathbf{1})]^{3+}$ (Fig. 1). Such finding suggests that the positive charge at the silver(I) is less neutralized by the BF$_4^-$ counter anion in $[\mathrm{Ag}_3(\mathbf{1})(\mathbf{2})]^{3+}$ than in $[\mathrm{Ag}_3(\mathbf{1})]^{3+}$, because motion in the former impedes close ion pairing.

Upon addition of **3** to $[\mathrm{Ag}_3(\mathbf{1})(\mathbf{2})]^{3+}$, the four-component slider-on-deck $[\mathrm{Ag}_3(\mathbf{1})(\mathbf{2})(\mathbf{3})]^{3+}$ was afforded as a stand-alone nano-assembly, as seen in the $^1$H NMR (Fig. 2) and ESI-MS (ESI,† Fig. S25). Since the proton signals of the phenanthroline core, 3-H, 4-H, 5-H, 6-H, 7-H and 8-H, exhibit identical shifts for

**Table 1** Yield of **6**, **8** and **10** furnished in presence of $[\mathrm{Ag}(\mathbf{3})]^+$ and $[\mathrm{Ag}(\mathbf{3})_2]^+$

| | Yield with $[\mathrm{Ag}(\mathbf{3})]^+$ | | | Yield with $[\mathrm{Ag}(\mathbf{3})_2]^+$ | | |
|---|---|---|---|---|---|---|
| Time (h) | Of **8** (Ag$^+$ cat.) (%) | Of **6** (base cat.) (%) | Of **10** (%) | Of **8** (Ag$^+$ cat.) (%) | Of **6** (base cat.) (%) | Of **10** (%) |
| 2 | 6 | <1 | 1 | 0 | <1 | 1 |
| 7 | 38 | 6 | 2 | 2 | 7 | 7 |
| 14 | 68 | 11 | 4 | 9 | 13 | 11 |
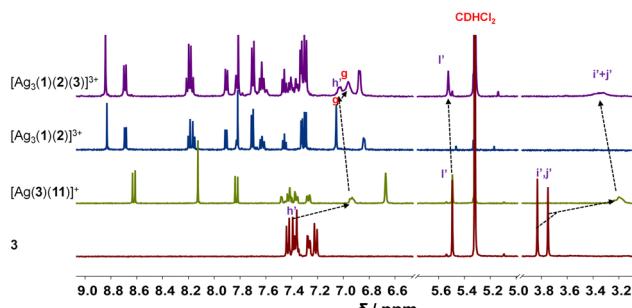
**Fig. 2** Comparison of partial $^1$H-NMR spectra (600 MHz, CD$_2$Cl$_2$, 298 K) of **3**, silver(I) phenanthroline complex [Ag(**3**)(**11**)]$^+$, three-component slider-on-deck [Ag$_3$(**1**)(**2**)]$^{3+}$, and four-component slider-on-deck [Ag$_3$(**1**)(**2**)(**3**)]$^{3+}$.

both slider-on-deck systems, one can deduce that [Ag$_3$(**1**)(**2**)(**3**)]$^{3+}$ is also in motion despite the addition of ligand **3**. By comparison of the shifts of proton signals i′, j′-H in **3** ($\delta_{i',j'}$ = 3.75, 3.83 ppm), [Ag$_3$(**1**)(**2**)(**3**)]$^{3+}$ ($\delta_{i',j'}$ = 3.33 ppm) and reference [Ag(**3**)(**11**)]$^+$ ($\delta_{i',j'}$ = 3.21 ppm), similar upfield shifts were observed for both complexes attesting that **3** is situated in the shielding pocket of the silver(I) phenanthroline sites (Fig. 2). As expected from product liberation in moving rotors,[13] ligand **3** in [Ag$_3$(**1**)(**2**)(**3**)]$^{3+}$ shows a shift that lies in between those of free **3** and [Ag(**3**)(**11**)]$^+$, indicating that some is liberated by the motion in the four-component slider-on-deck.

By means of variable temperature (VT) $^1$H NMR spectroscopy, we determined the exchange frequency of both slider-on-deck assemblies. In case of the three-component [Ag$_3$(**1**)(**2**)]$^{3+}$, the 4-H proton signal split at −60 °C into two peaks (ratio 2 : 1) due to freezing the sliding of biped **2** across deck **1** on the NMR time scale (Fig. 3). Using WinDNMR,[18] the $^1$H NMR traces were simulated over a large temperature range, providing the activation data as $\Delta H^\ddagger$ = 45.8 kJ mol$^{-1}$, $\Delta S^\ddagger$ = 0.7 J mol$^{-1}$ K$^{-1}$ and $\Delta G^\ddagger_{298}$ = 45.6 kJ mol$^{-1}$ as well as the exchange rate $k_{298}$ = 57 kHz. Contrastingly, in the four-component slider-on-deck [Ag$_3$(**1**)(**2**)(**3**)]$^{3+}$, the proton 4-H signal split already at −40 °C. The kinetic analysis afforded $k_{298}$ = 45 kHz along with the activation data $\Delta H^\ddagger$ = 47.8 kJ mol$^{-1}$, $\Delta S^\ddagger$ = 5.4 J mol$^{-1}$ K$^{-1}$ and $\Delta G^\ddagger_{298}$ = 46.3 kJ mol$^{-1}$. As a result of the addition of **3** to [Ag$_3$(**1**)(**2**)]$^{3+}$, the motion thus slowed down by 21% at room temperature and even more at lower temperature. This trend is
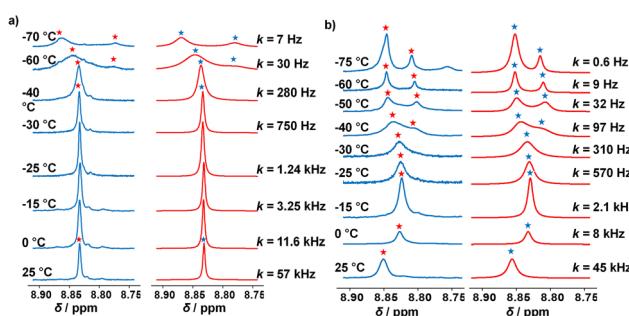
**Table 2** Product yield in both concurrent and sequential reactions catalyzed by [Ag$_3$(**1**)(**2**)(**3**)]$^{3+}$

| Time (h) | Yield of **6** (base cat.) (%) | Yield of **8** (Ag$^+$ cat.) (%) | Yield of **10** (dual seq. cat.) (%) |
|---|---|---|---|
| 0 | 0 | 0 | 0 |
| 2 | 7 | 17 | 2 |
| 4 | 18 | 35 | 7 |
| 6 | 25 | 47 | 12 |
| 8 | 29 | 53 | 15 |
| 10 | 33 | 61 | 21 |
| 12 | 35 | 64 | 27 |
| 14 | 38 | 67 | 34 |

a result of the higher positive activation entropy of [Ag$_3$(**1**)(**2**)(**3**)]$^{3+}$ that is increased due to the liberation of **3** into solution in the rate-determining step. As in the rate-limiting step the biped must depart from one silver(I) binding site to kick out the base **3**, both the silver(I) and **3** are temporarily available for catalysis.

To investigate whether both catalytic units in [Ag$_3$(**1**)(**2**)(**3**)]$^{3+}$ are simultaneously active we tested for concurrent base and silver(I) catalysis. Thus, the slider-on-deck [Ag$_3$(**1**)(**2**)(**3**)]$^{3+}$ and reactants **4**, **5**, and **7** were combined (1 : 30 : 30 : 30) in CD$_2$Cl$_2$ for running both transformations parallel (Scheme 2a). The reactions were monitored by $^1$H NMR over 14 h at room temperature, showing formation of the silver(I)-catalyzed product **8** (67%) and base-catalyzed product **6** (38%) as displayed in Table 2. The data demonstrate that the base-catalyzed formation of **6** is slower than the silver-catalyzed reaction affording **8**.

Since dual activity of this slider-on-deck is increased in comparison with the static model compounds, we probed a concurrent tandem catalysis consisting of a Michael addition followed by hydroalkoxylation (see Scheme 2b). Hence, the slider-on-deck [Ag$_3$(**1**)(**2**)(**3**)]$^{3+}$ and reactants **4** & **9** (1 : 30 : 30) were mixed in CD$_2$Cl$_2$. The kinetic profile of this reaction was monitored at room temperature by $^1$H NMR over 14 h at 2 h intervals. $^1$H NMR spectra showed 34% of **10** after 14 h (black curve in Fig. 4).

Closer inspection revealed several surprising features. Initially, the base catalyzed reaction is the rate-determining step in the tandem reaction to **10**, because intermediate **10**′ created by



**Fig. 3** Experimental (left) and simulated (right) partial VT $^1$H NMR spectra (CD$_2$Cl$_2$, 600 MHz) of (a) [Ag$_3$(**1**)(**2**)]$^{3+}$ and (b) of [Ag$_3$(**1**)(**2**)(**3**)]$^{3+}$.
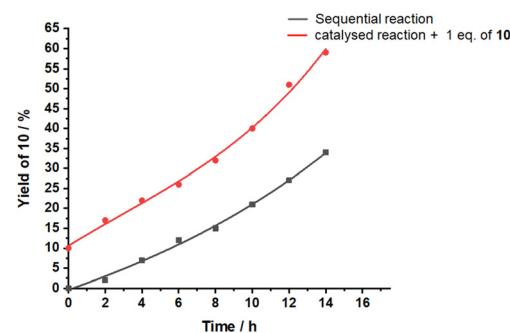


**Fig. 4** Yield of **10** with time in the tandem reaction catalysed by [Ag$_3$(**1**)(**2**)(**3**)]$^{3+}$.

base catalysis does not show up in the $^1$H NMR. Only, when product **10** of the tandem base- and silver(I) catalysis had formed to more than 15%, then intermediate **10′** (Scheme 2b) became visible. Furthermore, the kinetic profile of the tandem reaction showed an increasing rate the more product **10** had formed (Fig. 4), indicative of some autocatalytic effect. To check whether it is the final product **10** that impacts on the rate, the slider-on-deck $[Ag_3(\mathbf{1})(\mathbf{2})(\mathbf{3})]^{3+}$, reactants **4**, **9** and product **10** were mixed in a 1 : 30 : 30 : 3 ratio in $CD_2Cl_2$. Now 59% of **10** (49% after subtracting 10% of the initially added **10**) was afforded after 14 h with higher rate (initial rate at $t = 0$: $\nu_0 = 2.8\ \mu M\ s^{-1}$) than in absence of product **10** ($\nu_0 = 2.1\ \mu M\ s^{-1}$) (Fig. 4). This effect is attributed to the competitive displacement of base **3** at the silver(I)-loaded phenanthroline by product **10** as it may act as ligand as well. Thus, in presence of sliding motion and 1 equiv. of **10**, more base **3** is released.

In conclusion, we report a three-component slider-on-deck assembly $[Ag_3(\mathbf{1})(\mathbf{2})]^{3+}$ with a sliding speed of $k_{298} = 57$ kHz. Addition of amine **3** to the slider-on-deck converted it into a four-component dual-catalyst machinery $[Ag_3(\mathbf{1})(\mathbf{2})(\mathbf{3})]^{3+}$ with a reduced sliding speed ($k_{298} = 45$ kHz). The sliding motion in the machinery instigated two simultaneous events that enabled concurrent tandem catalysis: (a) liberation of base **3**, and (b) exposure of the silver(I) sites, so that they could act synergistically[19] as dual catalyst in the two-step synthesis of **10**. Thus, the present system portrays a lucid example of unleashing multiple catalytic functions instigated by a single nanomechanical motion within artificial catalytic machinery.

## Conflicts of interest

There are no conflicts to declare.

## Notes and references

1 Y. Huang, A. M. Walji, C. H. Larsen and D. W. C. MacMillan, *J. Am. Chem. Soc.*, 2005, **127**, 15051–15053.

2 J.-C. Wasilke, S. J. Obrey, R. T. Baker and G. C. Bazan, *Chem. Rev.*, 2005, **105**, 1001–1020.

3 P. Ojeda-May, A. U. Mushtaq, P. Rogne, A. Verma, V. Ovchinnikov, C. Grundström, B. Dulko-Smith, U. H. Sauer, M. Wolf-Watz and K. Nam, *Biochemistry*, 2021, **60**, 2246–2258.

4 M. J. Wiester, P. A. Ulmann and C. A. Mirkin, *Angew. Chem., Int. Ed.*, 2011, **50**, 114–137.

5 K. A. Henzler-Wildman, V. Thai, M. Lei, M. Ott, M. Wolf-Watz, T. Fenn, E. Pozharski, M. A. Wilson, G. A. Petsko, M. Karplus, C. G. Hübner and D. Kern, *Nature*, 2007, **450**, 838–844.

6 P. Neupane, S. Bhuju, N. Thapa and H. K. Bhattarai, *Biomol. Concepts*, 2019, **10**, 1–10.

7 (a) Z. Dong, Q. Luo and J. Liu, *Chem. Soc. Rev.*, 2012, **41**, 7890–7908; (b) M. Raynal, P. Ballester, A. Vidal-Ferran and P. W. N. M. van Leeuwen, *Chem. Soc. Rev.*, 2014, **43**, 1734–1787; (c) D. Zhang, T. K. Ronson and J. R. Nitschke, *Acc. Chem. Res.*, 2018, **51**, 2423–2436; (d) N. Mittal, M. S. Özer and M. Schmittel, *Inorg. Chem.*, 2018, **57**, 3579–3586; (e) F. J. Rizzuto, L. K. S. von Krbek and J. R. Nitschke, *Nat. Rev. Chem.*, 2019, **3**, 204–222; (f) G. Olivo, G. Capocasa, D. Del Giudice, O. Lanzalunga and S. Di Stefano, *Chem. Soc. Rev.*, 2021, **50**, 7681–7724; (g) P. Howlader and M. Schmittel, *Beilstein J. Org. Chem.*, 2022, **18**, 597–630; (h) A. W. Heard, J. M. Suárez and S. M. Goldup, *Nat. Rev. Chem.*, 2022, **6**, 182–196; (i) R. Saha, B. Mondal and P. S. Mukherjee, *Chem. Rev.*, 2022, **122**, 12244–12307.

8 *Supramolecular Catalysis: New Directions and Developments*, ed. P. W. N. M. van Leeuwen and M. Raynal, Wiley-VCH GmbH, Weinheim, 1st edn, 2022, ISBN: 9783527349029.

9 (a) N. Mittal, S. Pramanik, I. Paul, S. De and M. Schmittel, *J. Am. Chem. Soc.*, 2017, **139**, 4270–4273; (b) Y. Li, X. Caumes, M. Raynal and L. Bouteiller, *Chem. Commun.*, 2019, **55**, 2162–2165; (c) E. Iniesta and A. Vidal-Ferran, *Chem. Commun.*, 2020, **56**, 6364–6367.

10 L. van Dijk, M. J. Tilby, R. Szpera, O. A. Smith, H. A. P. Bunce and S. P. Fletcher, *Nat. Rev. Chem.*, 2018, **2**, 1–18.

11 V. V. Rajasekaran, A. Ghosh, S. Kundu, D. Mondal, T. Paululat and M. Schmittel, *Angew. Chem., Int. Ed.*, 2022, **61**, e2022124.

12 I. Paul, A. Goswami, N. Mittal and M. Schmittel, *Angew. Chem., Int. Ed.*, 2018, **57**, 354–358.

13 P. K. Biswas, S. Saha, T. Paululat and M. Schmittel, *J. Am. Chem. Soc.*, 2018, **140**(29), 9038–9041.

14 S. Gaikwad, A. Goswami, S. De and M. Schmittel, *Angew. Chem., Int. Ed.*, 2016, **55**, 10512–10517.

15 S. De, S. Pramanik and M. Schmittel, *Angew. Chem., Int. Ed.*, 2014, **53**, 14255–14259.

16 E. Elramadi, A. Ghosh, I. Valiyev, P. K. Biswas, T. Paululat and M. Schmittel, *Chem. Commun.*, 2022, **58**, 8073–8076.

17 U. Kaya, P. Chauhan, K. Deckers, R. Puttreddy, K. Rissanen, G. Raabe and D. Enders, *Synthesis*, 2016, 3207–3216.

18 H. J. Reich, *NMR Spectrum Calculations: WinDNMR, Version 7.1.13*, Department of Chemistry, University of Wisconsin.

19 L. Zhou and L. Liu, *Chem. Commun.*, 2021, **57**, 5690–5693.